Geoscience Letters

RESEARCH LETTER

Open Access

Dynamic conditions for large shallow intraslab earthquakes: four categories of subduction zones

Masaki Yoshida[1*]

Abstract

Large shallow intraslab earthquakes (LSIEs) of over magnitude-7 rarely occur at shallower depths (≤ 60 km) in the subducting plates of the circum-Pacific and northern margin of the Australian Plate off Indonesia. Previous studies have suggested that most LSIEs occur under surface tectonic conditions with a lateral stress gradient across the back-arc to the fore-arc on the overriding plate based on seismological and geological evidence. In this study, dynamic conditions for the occurrence of LSIEs were studied using the intraslab stress state, stress state of the overriding plate, motion speed of overriding and subducting plates, and trench migration speed determined by plate motion models. LSIEs prefer tectonic conditions under (1) an extensional-to-neutral stress state in the back-arc, (2) a compressional stress state in the fore-arc, and (3) down-dip tension in the shallower part of the subducting plate. The results suggest that the Earth's subduction zones can be classified into four categories. This categorization is informed by the behavior of underlying mantle flow, i.e., the magnitude of slab suction flow in the mantle under the subducting plates, which is related to the degree of plate-slab coupling, and the scale of return flow in the mantle wedge under the overriding plates, which varies the combination of stress states in the fore-arc and back-arc.

Introduction

Large shallow intraslab earthquakes (LSIEs) of over magnitude-7 rarely occur at depths of ≤ 60 km (Preston et al. 2002; Seno and Yoshida 2004). More recently, A M_w 8.2 intraslab earthquake occurred in Chiapas, Mexico, on September 8, 2017 (Ye et al. 2017). Since LSIEs cause severe damage owing to the shallower depths of their epicenters, deep understanding of the mechanism of LSIEs can aid hazard assessments in areas near related subduction zones. Furthermore, the occurrence of LSIEs possibly depends on dynamic interactions between not only the subducting and overriding plates but also between these plates and underlying mantle flow. Therefore, the study of the dynamic conditions for LSIEs is key to understanding the relationship between the Earth's surface activity, which is directly observable, and the Earth's deep activity, which is not directly observable and indirectly studied by, for example, numerical simulations, seismic tomography, and geochemical analyses of mantle rocks.

Based on the focal mechanisms of earthquakes, slab stress, and the stress state of overriding plates near the 20 events listed by the Global CMT catalog (Dziewonski et al. 1981; Ekström et al. 2012) and individual studies, Seno and Yoshida (2004) concluded that LSIEs occur in tectonic environments with down-dip tension (DDT) in the shallower part of the subducting plate and extensional back-arc stress, except for a few events. However, their analyses were based on a dataset from seismological and geological evidence and not on geodetic observation of plate motion, and they did not clearly discuss the phenomenon in terms of the relationship between surface observation and underlying mantle dynamics.

*Correspondence:
Masaki Yoshida
masakiy@fc.ritsumei.ac.jp
[1] Department of Physical Sciences, College of Science and Engineering, Ritsumeikan University, 1-1-1 Noji-Higashi, Kusatsu, Shiga 525-8577, Japan

Geodetic information of plate motion is useful for estimating not only absolute velocity and motion but also the deformation rate of the plate interior near a trench. In particular, such geodetic information produces a quantitative estimation of the stress state of the subducting and overlying plates and complements information from geological observations and focal mechanisms (e.g., Lallemand et al. 2005, 2008). In this study, I investigated dynamic conditions for LSIEs using a dataset for the intraslab stress state, stress state of the overriding plate, motion speed of the overriding and subducting plates, and trench migration speed (i.e., trench advance or retreat) determined by geodesic observation.

Stress states in the back-arc and fore-arc regions

Seno and Yoshida (2004) studied events with depths of 20–60 km, because events at depths shallower than 20 km cannot be distinguished from outer-rise events, and those deeper than 60 km are caused by unbending processes in the elastic core of the plate (Engdahl and Scholz 1977) and thermal stress constrained by slab morphology (Hamaguchi et al. 1977). It should be noted that bending/unbending-related events can occur at wide depth ranges, including within 20–60 km, and there is no uniform depth distribution pattern across all subduction zones (e.g., Craig et al. 2022; Sippl et al. 2022). Therefore, excluding the effects of bending and unbending by limiting the analysis to earthquakes in the 20–60 km range may not be robust, but this study followed the definition used in the previous study (Seno and Yoshida 2004).

Table 1 is a modified list of LSIEs based on the study by Seno and Yoshida (2004) and updated information, and Fig. 1 shows the distributions and focal mechanisms of the LSIEs listed in Table 1. This list was constructed mostly from the studies by Preston et al. (2002) and Wong (2005) for the Cascadia Trench, Ye et al. (2017) for the Mexico Trench, Mallick et al. (2017) for the Sumatra–Andaman Trench, and Harada and Ishibashi (2008) for the Mariana Trench, in addition to information from the Global CMT catalog and other individual studies. The largest LSIEs were the 1994 Hokkaido–Toho–Oki Earthquake and the 1958 Etrofu–Oki Earthquake, which occurred in the Kuril Trench, with a magnitude of 8.3. Although the latter was considered to be an interplate earthquake (Utsu 1972), more recent seismic analyses have suggested that this was an intraslab earthquake (Harada and Ishibashi 2000).

Based on the data base by Heuret and Lallemand (2005) and Lallemand et al. (2005), Lallemand et al. (2008) presented the absolute velocity of the subducting plates, overriding plates, and trench migration (V_{sub}, V_{up}, and V_t, respectively) on 166 transects at every 2° along subduction zones based on the three reference frames of plate motion, i.e., HS3 (Gripp and Gordon 2002), SB04 (Becker 2006; Steinberger et al. 2004), and NNR (DeMets et al. 1994; Gripp and Gordon 2002). Figure 2a, b demonstrate diagrams relating to trenches in HS3 reference frame, in which the velocities of the subducting plate (V_{sub}) versus those of overriding plate (V_{up}) for 166 trenches (Fig. 2a) and trenches where the large shallow intraslab earthquakes (LSIEs) occur (Fig. 2b) were plotted. The green, gray, and orange circles show the extensional, neutral, and compressional stress regimes in the back-arc as deduced from focal mechanisms of earthquakes following the work of Heuret and Lallemand (2005) and Lallemand et al. (2008). Following their definitions, the extensional stress state is characterized by dominant normal focal mechanisms with strike-slip components, whereas the compressional stress state is characterized by dominant reverse focal mechanisms with strike-slip components. The "neutral" stress state indicates the focal mechanism region characterized by dominant strike-slip or no earthquakes within the overriding plate (see Heuret and Lallemand (2005) for details).

Meanwhile, Heuret and Lallemand (2005) defined the stress regimes inferred from the above geodetic data in the back-arc region, independently of the focal mechanism. In their definition, the relative value of back-arc deformation is defined by

$$v_d \equiv V_t - V_{up}, \tag{1}$$

where negative and positive v_d values indicate back-arc compression (i.e., shortening) and extension (i.e., spreading), respectively (Fig. 3).

In this paper, the relative value of fore-arc deformation was newly defined by

$$v_c \equiv V_{sub} - V_{up}, \tag{2}$$

where negative and positive v_c values indicate fore-arc compression (i.e., shortening) and extension (i.e., spreading) respectively (Fig. 3). To determine the relationship between the back- and fore-arc stress states, I plotted v_d-versus-v_c diagrams of the 166 trenches in the three reference frames (Fig. 2c and Figs. S1c and S2c in the supplementary material). On the other hand, Fig. 2d and Figs. S1d and S2d in the supplementary material show the v_d-versus-v_c diagram of trenches where LSIEs occur; I identified 47 trenches relating to LSIEs, including the Sumatra, Andaman, Manila (Luzon), Mariana, Kuril, Alaska, Cascadia, Mexico, Costa Rica, Peru, Northern Chile, and New Hebrides Trenches as well as the Nankai Trough (Table 1). These 47 trenches include 13, 25, and 9 trenches of compressional, neutral, and extensional regimes in the back-arc, respectively, as deduced from

Table 1 List of large shallow intraslab earthquakes

No	Event	Trench	Origin (year/month/day)	Epicenter		M_W	d	Faulting parameter			Slab age	References
				Lat	Lon			φ	δ	λ		
1	Sumatra	Sumatra	2000/06/04	−4.73	101.94	7.8	44	92	55	152	60–72	Seno and Yoshida (2004)
2	Sumatra	Andaman	2010/06/12	7.85	91.65	7.5	33	115	63	149	69–86	Mallick et al. (2017)
3	Manila	Manila (Luzon)	1999/12/11	15.87	119.64	7.2	35	112	13	−169	18–32	Seno and Yoshida (2004)
4	Kii-Yamato	Nankai	1899/03/07	34.1	136.1	7.0	45	–	–	–	17–21	Utsu (1982)
5	Geiyo		2001/03/24	34.13	132.71	6.8	47	181	57	−67		Preston et al. (2002); Seno and Yoshida (2004)
6	Geiyo		1905/01/02	34.1	132.5	7.2	50	–	–	–		Utsu (1982)
7	Yoshino		1952/07/18	34.5	135.8	6.8	60	–	–	–		Utsu (1982)
8	Hyuganda		1931/11/02	32.2	132.1	7.1	40	–	–	–		Utsu (1982)
9	Guam	Mariana	1993/08/08	12.98	144.80	7.7	45	238	24	82	156	Harada and Ishibashi (2008)
10	Hokkaido-Toho-Oki	Kuril	1994/10/04	43.42	146.81	8.3	33	158	41	24	118–128	Utsu (1982)
11	Etorofu-Oki		1958/11/07	44.38	148.58	8.3	32	–	–	–		Harada and Ishibashi (2000)
12	Kodiak Is	W. and E. Alaska	1999/12/06	57.35	−154.35	7.0	36	357	63	−180	40–52	Utsu (1982)
13	Nisqually	Cascadia	2001/02/28	47.14	−122.53	6.8	47	176	17	−96	10–11	Preston et al. (2002); Wong (2005)
14	Seattle-Tacoma		1965/04/29	47.38	−122.31	6.7	60	344	70	−75		Preston et al. (2002); Wong (2005)
15	Olympia		1949/04/13	47.17	−122.62	7.1	54	14	82	−135		Baker and Langston (1987); Preston et al. (2002); Wong (2005)
16	Chiapas	Mexico	2017/09/08	15.34	−94.62	8.2	50	148	13	−83	8–15	Ye et al. (2017)
17	Oaxaca		1999/09/30	15.70	−96.96	7.4	47	102	42	−103		Ye et al. (2017)
18	Oaxaca		1931/01/15	16.4	−96.3	7.7	40	90	34	−90		Ye et al. (2017)
19	Oaxaca		1907/04/15	16.51	−97.30	7.6	30	–	–	–		Ye et al. (2017), USGS
20	Michoacán		1997/01/11	18.34	−102.58	7.1	40	175	18	−28		Seno and Yoshida (2004)
21	Guerrero		1957/07/28	17.06	–99.09	7.6	38	–	–	–		Ye et al. (2017), USGS
22	El Salvador	Costa-Rica	1982/06/19	12.65	−88.97	7.3	52	102	25	−106	22–28	Seno and Yoshida (2004)
23	El Salvador		2001/01/13	12.97	−89.13	7.7	56	121	35	−95		Preston et al. (2002)
24	Peru	Peru	1970/05/31	−9.18	−78.82	7.9	43	160	37	−90	31–46	Abe (1972)
25	Taltal	N. Chile	1965/02/23	−25.67	−70.79	7.0	60	16	86	−78	52–53	Utsu (1982)
26	Vanuatu	S. and. N. New Hebrides	1994/07/13	−16.50	167.35	7.1	25	272	42	2	45–60	Utsu (1982)
27	Vanuatu		1981/07/06	−22.31	170.90	7.5	58	345	30	−179		Utsu (1982)

Symbols: d: depth; δ: dip; λ: rake; φ: strike

USGS: webpage of United States Geological Survey

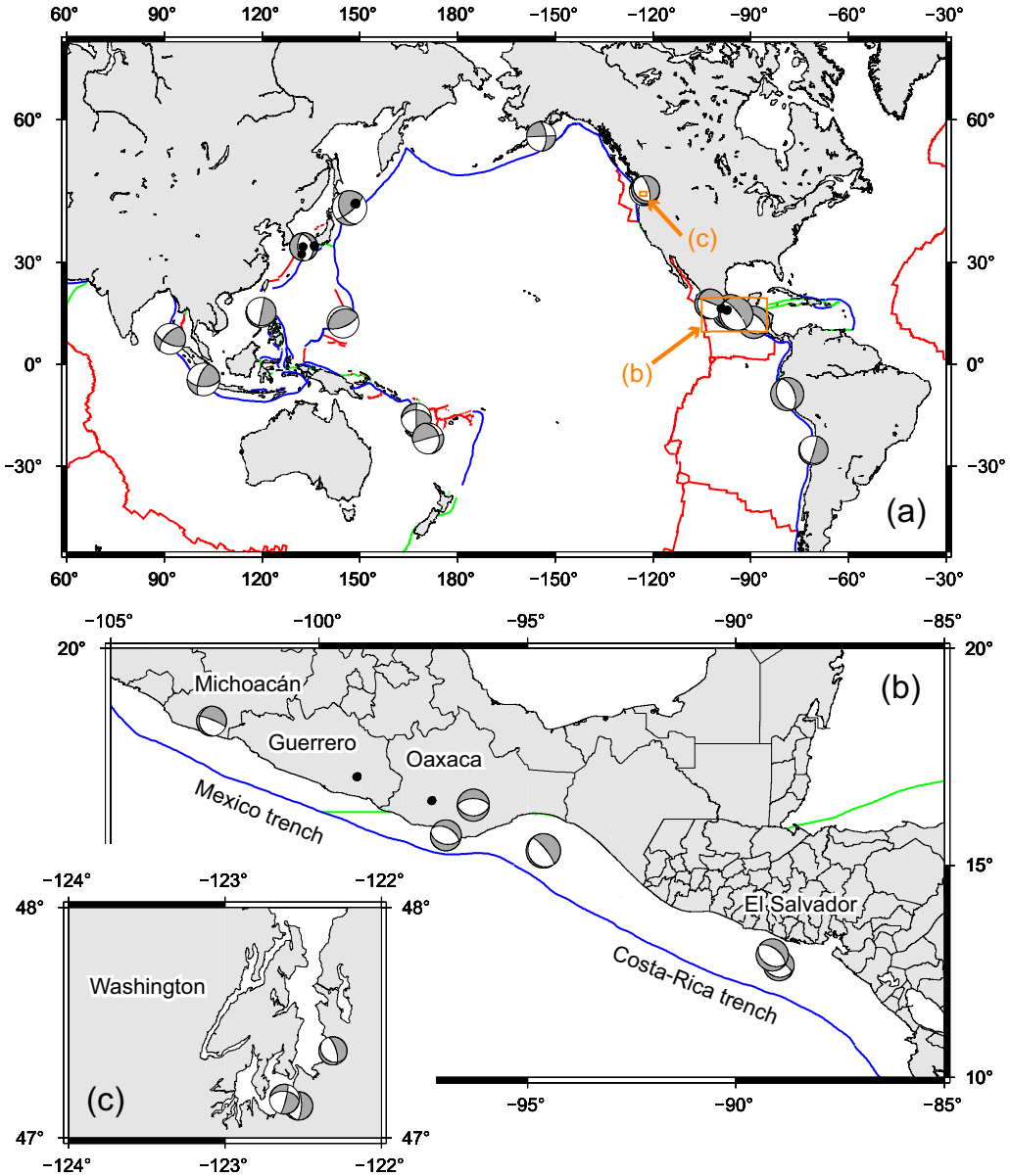

Fig. 1 **a** Distributions and focal mechanisms of the large shallow intraslab earthquakes listed in Table 1. **b** Close-up view around the Mexico and Costa-Rica Trenches shown by a small orange rectangle in (**a**). **c** Close-up view of a part of Washington, United States, shown by an orange rectangle in (**a**). Blue, green, and red lines indicate the trenches, transform-faults, and ridges, respectively

research on the focal mechanisms of earthquakes (Lallemand et al. 2005, 2008).

It was found that the distribution of these plots did not depend on the reference frames significantly, although the V_{sub}-versus-V_{up} diagrams (Fig. 2a and Figs. S1a and S2a in the supplementary material) and the V_{sub}-versus-V_t diagram (Fig. 2b and Figs. S1b and S2b in the supplementary material) show variations in the three reference frames. Because the velocities of the subducting and overriding plates and the speed of trench migration in each trench depend on the reference frame (e.g., Heuret and Lallemand 2005; Schellart et al. 2008), it was difficult to quantitatively determine the effects of the relative plate motion of the subducting and overriding plates on the stress states of the back- and fore-arcs. Therefore, I focused only on the dynamic conditions for LSIEs in terms of the relationship between the back- and fore-arc stress states from the geodetic data and intraslab stress from the focal mechanisms.

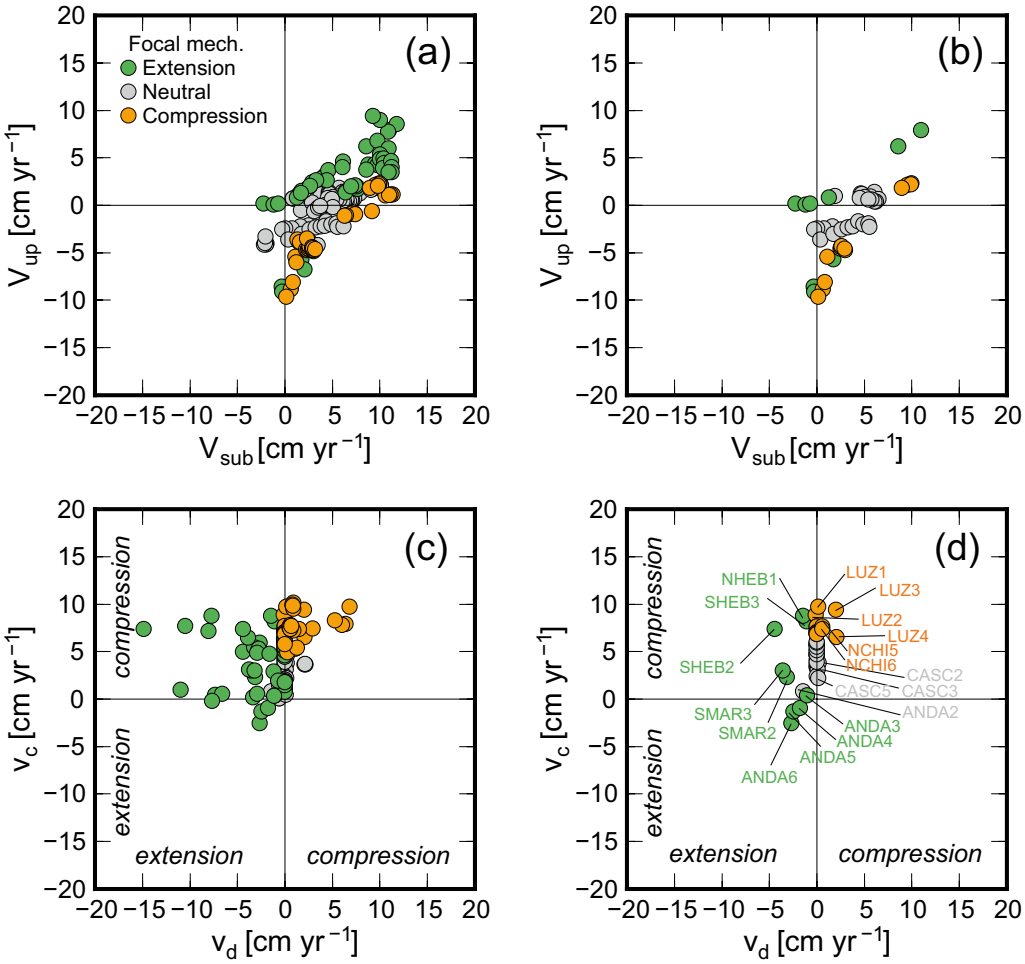

Fig. 2 Diagrams relating to trenches in HS3 reference frame (Gripp and Gordon 2002). **a** and **b** Velocities of the subducting plate (V_{sub}) versus those of overriding plate (V_{up}) for **a** 166 trenches and **b** trenches where the large shallow intraslab earthquakes (LSIEs) occur. (c and d) Back-arc deformation (v_d) versus fore-arc deformation (v_c) for **c** 166 trenches and **d** trenches where LSIEs occur. Green, gray, and orange circles show the extensional, neutral, and compressional stress regimes in the back-arc as deduced from focal mechanisms of earthquakes following the work of Lallemand et al. (2008). Abbreviations in **d**: SHEB#: southern New Hebrides Trench; NHEB#: northern New Hebrides Trench; ANDA#: Andaman Trench; SMAR#: southern Mariana Trench; LUZ#: Manila (Luzon) Trench; NCHI#: Northern Chile Trench; CASC#: Cascadia Trench (where "#" is the number indicating each transect across the trenches; see Table 1 of Lallemand et al. (2008))

Figure 2d demonstrates that LSIEs are found for a wide range of v_d values, varying from −4.44 cm yr^{-1} to + 2.06 cm yr^{-1}, and many trenches (28 of 47) are neutral, i.e., $v_d = 0.0$ cm yr^{-1}. On the other hand, the 10 trenches with $v_d < 0$ are a part of the southern and northern New Hebrides, southern Mariana, and Andaman Trenches, which are minor compared to other trenches in the Western Pacific and northern Australian Plate off Indonesia. The five trenches with $v_d > 0$ are a part of the Manila (Luzon) and Northern Chile Trenches, which are relatively minor compared to other major trenches. Therefore, I concluded that LSIEs prefer tectonic conditions under (1) an extensional-to-neutral stress state in the back-arc and (2) a compressional stress state in the fore-arc from the present analyses. Furthermore, LSIEs prefer tectonic conditions under (3) DDT in the shallower part of the subducting plate, as previously suggested by Seno and Yoshida (2004).

Four categories of subduction zones

Subduction zone systems have geological, seismological, and geodynamic characteristics. For example, Conrad et al. (2004) classified trenches in subduction zone systems into two types in terms of the mechanical coupling between the surface and subducting plates ("plate-slab coupling"). One type includes trenches under conditions with a strong mechanical coupling between these plates, such as the South Chile, Aleutian, and Japan,

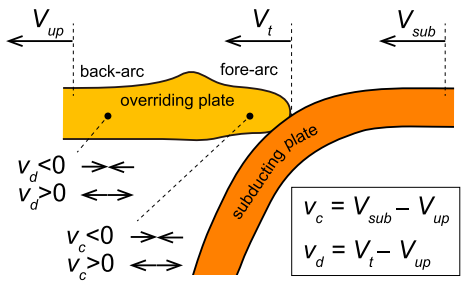

Fig. 3 Definitions of the velocity of the overriding plate (V_{up}), subducting plate (V_{sub}), and speed of trench migration (V_t) following the work of Lallemand et al. (2008). Negative and positive values of back-arc (v_d) and fore-arc (v_c) deformations show extension (i.e., spreading) and compression (i.e., shortening), respectively. The capital letter "*V*" indicates the speed from the observation and the lower-case letter "*v*" indicates the relative speed estimated from the observation. Note that $V_{up} \sim V_t$ in many trenches (Lallemand et al. 2008)

and Kuril–Kamchatka Trenches (Fig. 6a of Conrad et al. (2004)). In this type of subduction zone system, the slab pull force is decoupled or weakly coupled with the surface plate, because the convergent continent–ocean margin is considered to be mechanically damaged in the shallower part of the subducting slab. The other type includes trenches under conditions with a weak mechanical coupling between them, such as the Tonga–Kermadec, Java–Andaman, and Izu–Bonin (Ogasawara)–Mariana Trenches (Fig. 6b of Conrad et al. (2004)). In this type, the slab pull force is strongly coupled with the surface plate because there is no mechanical damage in the shallower part of subducting slab when the continental plate moves backward from the trench (see Yoshida (2017) for details).

The above classification is used in Fig. 4 to demonstrate the proposed four categories of subduction zone systems in terms of the back- and fore-arc stress states, magnitudes of slab suction flow under the subducting plates and mantle wedge flow under the overriding plates, and intraslab stress state in the subducting plate (see also Fig. S3 in the supplementary material). The latter from the focal mechanism has been discussed in previous studies (Alpert et al. 2010; Bailey et al. 2012; Goes et al. 2017; Isacks and Molnar 1971). The categories in Figs. 4c, d are similar to those in Figs. 6a, b of Conrad et al. (2004), respectively, but are slightly different, for example, the back-arc in the Japan Trench shows a compressional stress state, whereas that in the Aleutian Trench has a neutral stress state; the back-arc stress in Fig. 4d is indicated by "C ~ N". LSIEs are expected to occur in the subduction zone systems of Types I and II and not to (or to hardly) occur in those of Types III and IV. Indeed, in Type III (Fig. 4c), a magnitude-9 mega-trench earthquake has not occurred in the Izu–Bonin (Ogasawara)–Mariana and Tonga Trenches since at least 1700 CE (McCaffrey 2008).

The intraslab stress is related to the morphology of the subducting plate in the mantle. According to the seismic tomography model focused on the Cascadia Trench (e.g., Hawley et al. 2016; Obrebski et al. 2010), the Mexico and Costa Rica Trenches (e.g., Li et al. 2008), and the Nankai Trough (e.g., Huang et al. 2013), high seismic velocity regions in the shallower lower mantle—indicating the morphology of the subducting plate—do not directly reach the highly viscous lower mantle and are not subject to resistance forces from the lower mantle, which generates DDT in the shallower part of the subducting plate. LSIEs seem to occur frequently in these trenches, as classified as Type II in this paper.

In 2000, an LSIE occurred near the southernmost part of the Sumatra Trench. High-resolution seismic tomography demonstrated that the subducting Indian Plate penetrates the shallower lower mantle at a depth of approximately 1000 km (Li et al. 2008; Zahirovic et al. 2014) and does not appear to stagnate in the mantle transition zone, which is consistent with the fact that the intraslab stress shows DDT because the slab is not subjected to resistance forces from the lower mantle. Therefore, the dynamic condition in the southernmost part of the Sumatra Trench was classified as Type I in this paper (Fig. 4a).

On the other hand, in 2004, a megathrust earthquake occurred in the Andaman Trench, (M_w 9.3 Sumatra Earthquake), which is considered to be LSIE (Table 1). This trench shows back-arc spreading in the Andaman Sea (Diehl et al. 2013). High-resolution seismic tomography images showed that the subducting Indian Plate penetrated the lower mantle at a depth of approximately 1000 km (Li et al. 2008; Zahirovic et al. 2014), which is consistent with the fact that the intraslab stress showed DDT. Because the largest part of the Andaman Trench has fore- and back-arc extension (Fig. 2d), the Andaman Trench was grouped into Type II in this study (Fig. 4b).

For the Japan Trench, a magnitude-9 class megathrust earthquake should not occur from a classical "comparative subductology" perspective (Uyeda and Kanamori 1979), but in 2011 a M_w 9.0 earthquake occurred off the Pacific coast of Tohoku. An LSIE has not been confirmed in the Japan Trench in recorded history. In this paper, the Japan Trench was classified as Type IV (Fig. 4d), where the coupling between plate and slab is weak. The intraslab stress is neutral and an LSIE should not occur in the Japan Trench, as well as in the Aleutian Trench, because the flattened slab with a lateral width

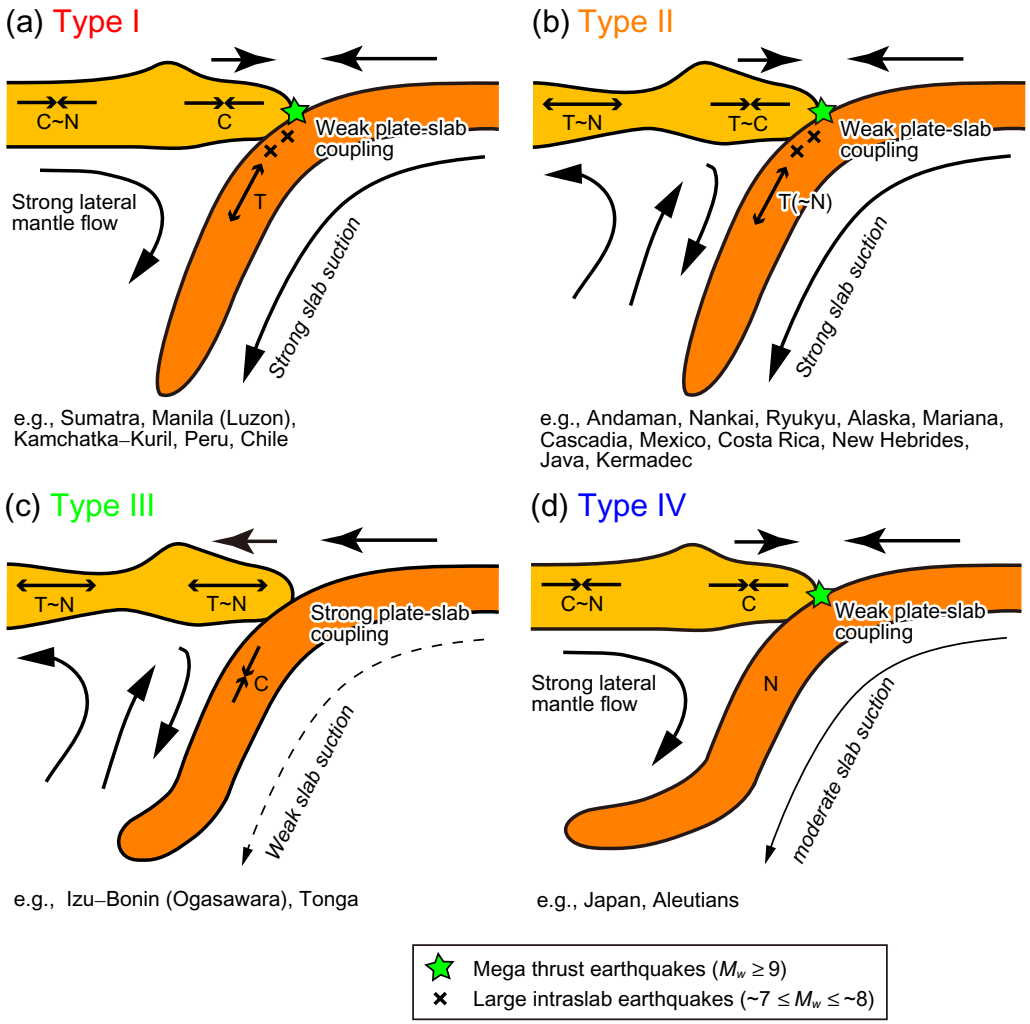

Fig. 4 Categories showing the relationship between the intraslab and arc stress, and the occurrence of large shallow intraslab earthquakes (LSIEs) and magnitude-9 class megathrust earthquakes. **a** Subducting slab shows down-dip tension (DDT) in the shallower part and the arc shows broadly compressional stress field, e.g., the Sumatra, Manila (Luzon), Kamchatka–Kuril, Peru, and Chile Trenches. **b** Subducting slab shows DDT in the shallower part and the arc shows an extensional-to-neutral stress field in the back-arc, e.g., the Andaman, Ryukyu, Alaska, Mariana, Cascadia, Mexico, Costa Rica, New Hebrides, Java, and Kermadec Trenches, as well as the Nankai Trough. **c** Subducting slab shows down-dip compression (DDC) in the shallower part and the arc shows broadly extensional-to-neutral stress field, e.g., the Izu–Bonin (Ogasawara) and Tonga Trenches. **d** Subducting slab shows neutral stress in the shallower part, and the arc shows compressional-to-neutral stress field in the back-arc, and compressional stress field in the fore-arc, e.g., the Japan and Aleutian Trenches. The outward-pointing arrows with abbreviation "T" indicate the extensional stress field, the inward-pointing arrows with abbreviation "C" indicate the compressional stress field, and the abbreviation "N" indicates the neutral stress state. LSIEs may occur in Types I and II, whereas it is unlikely to occur in Types III and IV

of more than 1000 km is formed around the base of the mantle transition zone (e.g., Zhao 2015).

Figure 5 shows the result of a three-dimensional numerical simulation of mantle convection with plate subduction based on a model of Yoshida (2013) and Tajima et al. (2015), whose dynamic situation is assumed to be the Japan Trench. Moderately strong slab suction flow under the subducting plate and strong lateral mantle flow in the mantle wedge are generated because the subducting plate stagnates around the base of the mantle transition zone. Furthermore, the calculated surface stress state shows fore- and back-arc compression. This dynamic situation was grouped into Type IV (Fig. 4d). The strong mantle flow in the mantle wedge enhances the spontaneous retreat of the subducting plate and the flattening of the subducting plate in the mantle transition zone (Yoshida 2017). In contrast, if the strong mantle flow in the mantle wedge does not exist in the mantle wedge, the flattening of the subducting plate in the mantle transition zone does not

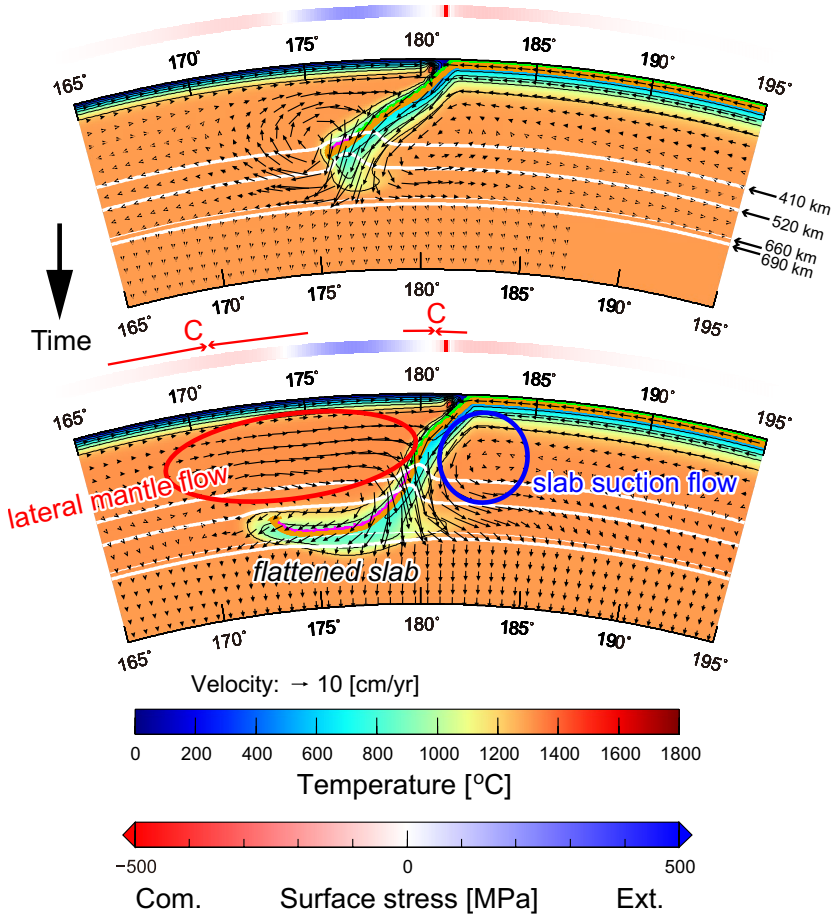

Fig. 5 Snapshots from the numerical simulation of mantle convection with slab subduction based on the model of Yoshida (2013) (For the model setup, see Yoshida (2013) and Tajima et al. (2015)). The upper color bar indicates the temperature in the model region, and the lower one indicates the surface stress (red and blue means compressional and extensional stress, respectively). The model setup and the dynamics situation are similar to Type IV in Fig. 4d. The red and blue circles respectively show strong horizontal mantle flow in the mantle wedge under the overriding plate and slab suction flow under the subducting plate. The outward-pointing arrows marked "C" indicate the fore- and back-arc compression

occur. Therefore, the flattened slab may not be observed in the dynamic situation with extensional stress in the overriding plate ("No" in Fig. S3 in the supplementary material).

The slab suction flow generated by plate subduction is not directly related to the surface deformation on the overriding plate and the mechanical coupling between the overriding and subducting plates. On the other hand, the horizontal scale and magnitude of the mantle flow under the overriding plate are assumed to be related to the surface deformation on the overriding plate. When the lateral scale of the mantle flow is large and the magnitude of the flow velocity is large (Fig. 4a and d), the overriding plate is compressed towards the trench, whereas when the horizontal scale of the lateral mantle flow is relatively small (Fig. 4b and c), the surface deformation becomes complex and possibly the back- or forearc stresses become extensional and neutral, as demonstrated by numerical studies of subduction dynamics (e.g., Ishii and Wallis 2022).

Discussion

In this study, I evaluated dynamic conditions for LSIEs using a dataset for the intraslab stress state, stress state of the overriding plate, motion speed of the overriding and subducting plates, and trench migration speed using geodetic data of plate motion in contrast to the qualitative evaluation based on seismological and geological observations of trenches by Seno and Yoshida (2004). LSIEs occur in the Cascadia, Mexico, and Costa Rica Trenches as well as the Nankai Trough relatively often. Seno and Yoshida (2004) suggested that LSIEs occur in trench regions where the overriding plate shows a lateral stress gradient, and the Kuril, Manila (Luzon), and Sumatra Trenches were considered exceptions. The present study suggests that these trenches have compressional stress

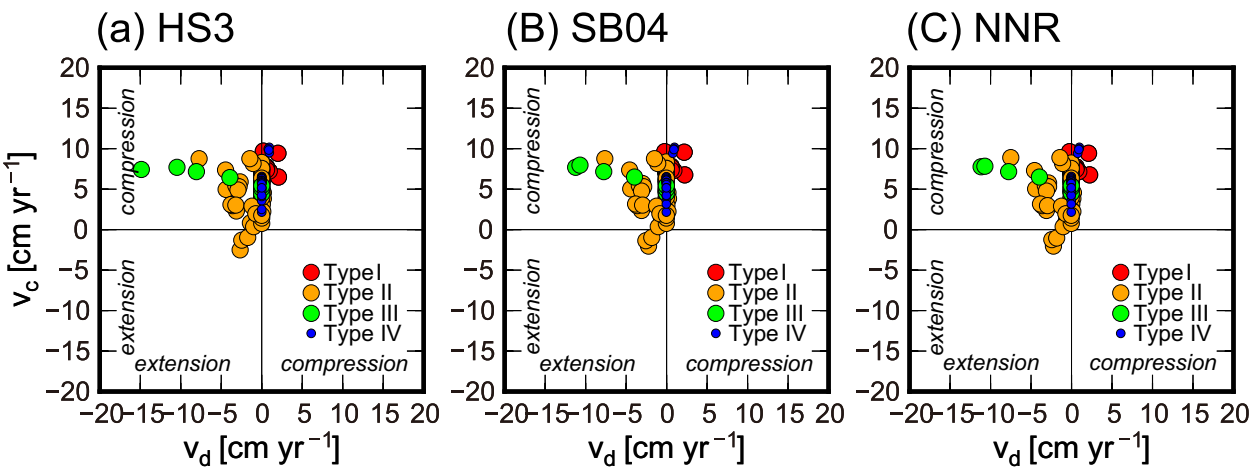

Fig. 6 Back-arc deformation (v_d) versus fore-arc deformation (v_c) for (**c**) 127 trenches in HS3 reference frame (Gripp and Gordon 2002), SB4 reference frame (Becker 2006; Steinberger et al. 2004), and NNR reference frame (DeMets et al. 1994; Gripp and Gordon 2002). The 127 trenches correspond to those shown in Fig. 4. The red, orange, green, and blue circles show Type I, II, III, and IV, respectively, in the four categories of subduction zones shown in Fig. 4

states in the fore-arc and nearly-neutral stress state in the back-arc, and were grouped into Type I in this paper (Fig. 4a).

Subduction zones have been classified into four types based on surface tectonic motions, stress states in back-arc and forearc regions, and mantle dynamics, providing preliminary suggestions for linking LSIEs and mantle/subduction dynamics (Fig. 4). Compared with Type I (Fig. 4a) and Type IV (Fig. 4d), and with Type II (Fig. 4b) and Type III (Fig. 4c), the stress states of the back-arc and fore-arc are similar. Thus, the nature of LSIEs depends mainly on the interaction between the properties of the subducting plates and the mantle transition zone.

Neither magnitude-9 megathrust earthquakes nor LSIEs have occurred in the Izu–Bonin (Ogasawara) and Tonga Trenches in recorded history. On the other hand, LSIEs have been confirmed near Gaum Island off the Mariana Trench (Table 1). In addition, Harada and Ishibashi (2008) reported that three earthquakes near Gaum Island on August 8, 1993 (depth = 67 km, M_w 7.8), October 12, 2001 (depth = 62 km, M_w 7.0), and April 26, 2002 (depth = 69 km, M_w 7.1) were taken as intraslab earthquakes, which occurred in the subducting Pacific Plate, and not as interplate earthquakes. Although the focal mechanisms of these three earthquakes showed DDT, even though the epicenter depths were slightly deeper than 60 km, the dynamic environments of these earthquakes can be explained by Type II (Fig. 4b). The difference between the Izu–Bonin (Ogasawara) and Mariana Trenches was attributed to the behavior of the subducting plate. The former trench stagnates at the base of the mantle transition zone, whereas the latter penetrates the 660 km phase boundary (e.g., Fukao and Obayashi 2013; Fukao et al. 2001). Thus, down-dip compression (DDC) appears in the slab under the Izu–Bonin (Ogasawara) Trench, whereas both DDT and DDC appear in the shallower and deeper parts of slabs in the Mariana Trench (Goes et al. 2017). In other words, it may be concluded that the morphology of the subducting plate in the mantle transition zone affects the possibility of an LSIE occurring.

In the New Britain Trench, the Ontong-Java Plateau, which is the largest oceanic plateau on Earth, collides with the Australia Plate. In this region, there is a strong coupling relationship between them, leading to a strong necking of the subducting plate, as shown by the numerical studies (Wang et al. 2022). Although an LSIE has not been confirmed in this trench in the recorded history, this subduction zone may be classified as Type II, because the focal mechanism shows that the back-arc stress is extensional (Lallemand et al. 2005, 2008).

The Java and Kermadec Trenches, where neither megathrust earthquakes (McCaffrey 2008) nor LSIEs have occurred in recorded history, have DDT in the shallower parts of the slabs (Alpert et al. 2010; Bailey et al. 2012; Goes et al. 2017; Isacks and Molnar 1971), and the focal mechanisms show a neutral back-arc in the Java Trench and back-arc extension in the Kermadec Trench (Lallemand et al. 2008). Therefore, these two trenches may be grouped into Type III (Fig. 4c).

The complex behavior of mantle flow under the overriding and subducting plates depends on the morphology of the subducting plate, amongst others. However,

the flattened slab around the base of the mantle transition zone can generate strong lateral flow in the mantle wedge, and the penetration of the subducting plate can generate slab suction flow under the subducting plate. Three-dimensional numerical simulations of mantle convection considering plate subduction may help to resolve these problems regarding deep mantle flow and the effects of mantle flow on the stress states in the subducting slab and overriding plate, but it is nevertheless difficult to simulate subduction dynamics in individual trenches even with modern computational power. For example, the high-resolution numerical model focused on the Japan Trench (Fig. 5), the surrounding tectonics of which are relatively simple, has a numerical resolution of ~ 8 km and ~ 9 km in the vertical and horizontal directions, respectively, which are insufficient for treating complex surface tectonics. Nonetheless, LSIEs can be key to a deeper understanding of the relationship between the surface observation and underlying mantle flow from the perspective of plate-slab coupling and interplate coupling in a solid-earth system, linking seismology and mantle dynamics.

Conclusions

This paper presented a statistical analysis exploring the dynamic conditions leading to large shallow intraslab earthquakes (LSIEs) with magnitudes over 7 at depths ranging from 20 to 60 km. This study integrated geodetic data, seismological data, and numerical simulations to understand the stress states and plate motions that influence LSIEs.

LSIEs prefer tectonic conditions under (1) an extensional-to-neutral stress state in the back-arc, (2) a compressional stress state in the fore-arc, and (3) down-dip tension in the shallower part of the subducting plate. The conclusions of (1) and (2) were not varied for three reference models of plate motion, i.e., HS3, SB04, and NNR (Fig. 6). The present results suggest that the Earth's subduction zones can be classified into four categories. This categorization is informed by the behavior of underlying mantle flow, i.e., the magnitude of slab suction flow in the mantle under the subducting plates, which is related to the degree of plate-slab coupling, and the scale of return flow in the mantle wedge under the overriding plates, which varies the combination of stress states in the fore-arc and back-arc.

Supplementary Information

The online version contains supplementary material available at https://doi.org/10.1186/s40562-024-00361-7.

Supplementary material: **Figure S1.** Same as Fig. 2 in the main text, but for SB4 reference frame. **Figure S2.** Same as Fig. 2 in the main text, but for NNR reference frame. **Figure S3.** Relationship between the relative plate motion, overriding plate stress, and intra-slab stress.

Acknowledgements
I would like to thank the Editor K. Satake and two anonymous reviewers for their careful reviews and thoughtful comments, which helped to improve the manuscript. Some figures were produced by using Generic Mapping Tools software (Wessel et al. 2013). The simulation shown in Fig. 5 was performed using the Earth Simulator (ES4) and the former supercomputer facility (DA system) at Japan Agency for Marine-Earth Science and Technology (JAMSTEC).

Author contributions
M.Y. solely contributed to the manuscript.

Funding
The author received no financial support for the research, authorship, and/or publication of this article.

Availability of data and materials
The datasets used and/or analyzed during the current study are available from the corresponding author on reasonable request.

Declarations

Competing interests
The author declares that they have no competing interests

Received: 18 June 2024 Accepted: 30 September 2024
Published online: 09 October 2024

References

Abe K (1972) Mechanics and tectonic implications of the 1966 and 1970 Peru earthquakes. Phys Earth Planet Sci 5:367–379. https://doi.org/10.1016/0031-9201(72)90108-2

Alpert LA, Becker TW, Bailey IW (2010) Global slab deformation and centroid moment tensor constraints on viscosity. Geochem Geophys Geosyst 11(12):Q12006. https://doi.org/10.1029/2010GC003301

Bailey IW, Alpert LA, Becker TW, Miller MS (2012) Co-seismic deformation of deep slabs based on summed CMT data. J Geophys Res 117(B4):B04404. https://doi.org/10.1029/2011JB008943

Baker GE, Langston CA (1987) Source parameters of the 1949 magnitude 7.1 south Puget Sound, Washington, earthquake as determined from long-period body waves and strong ground motions. Bull Seism Soc Am 77(5):1530–1557. https://doi.org/10.1785/BSSA0770051530

Becker TW (2006) On the effect of temperature and strain-rate dependent viscosity on global mantle flow, net rotation, and plate-driving forces. Geophys J Int 167(2):943–957. https://doi.org/10.1111/j.1365-246X.2006.03172.x

Conrad CP, Bilek S, Lithgow-Bertelloni C (2004) Great earthquakes and slab pull: interaction between seismic coupling and plate-slab coupling. Earth Planet Sci Lett 218(1–2):109–122. https://doi.org/10.1016/S0012-821X(03)00643-5

Craig TJ, Methley P, Sandiford D (2022) Imbalanced Moment Release Within Subducting Plates During Initial Bending and Unbending. J Geophys Res Solid Earth 127(3):e2021JB023658. https://doi.org/10.1029/2021JB023658

DeMets C, Gordon RG, Argus DF, Stein S (1994) Effect of recent revisions to the geomagnetic reversal time scale on estimates of current plate motions. Geophys Res Lett 21(20):2191–2194. https://doi.org/10.1029/94GL02118

Diehl T, Waldhauser F, Cochran JR, Kamesh Raju KA, Seeber L, Schaff D, Engdahl ER (2013) Bacl-arc extension in the Andaman sea: tectonic and magmatic processes imaged by high-precision teleseismic double-difference earthquake relocation. J Geophys Res 118(5):2206–2224. https://doi.org/10.1002/jgrb.50192

Dziewonski AM, Chou T-A, Woodhouse JH (1981) Determination of earthquake source parameters from waveform data for studies of global and regional seismicity. J Gepohys Res 86(B4):2825–2852. https://doi.org/10.1029/JB086iB04p02825

Ekström G, Nettles M, Dziewonski AM (2012) The global CMT project 2004–2010: centroid-moment tensors for 13,017 earthquakes. Phys Earth Planet Int 200–201:1–9. https://doi.org/10.1016/j.pepi.2012.04.002

Engdahl ER, Scholz CH (1977) A double Benioff zone beneath the central Aleutians: an unbending of the lithosphere. Geophys Res Lett 4(10):473–476. https://doi.org/10.1029/GL004i010p00473
Fukao Y, Obayashi M (2013) Subducted slabs stagnant above, penetrating through, and trapped below the 660 km discontinuity. J Geophys Res 118(11):5920–5938. https://doi.org/10.1002/2013JB010466
Fukao Y, Widiyantoro S, Obayashi M (2001) Stagnant slabs in the upper and lower mantle transition region. Rev Geophys 39(3):291–323. https://doi.org/10.1029/1999RG000068
Goes S, Agrusta R, van Hunen J, Garel F (2017) Subduction-transition zone interaction: a review. Geosphere 13(3):644–664. https://doi.org/10.1130/GES01476.1
Gripp AE, Gordon RG (2002) Young tracks of hotspots and current plate velocities. Geophys J Int 150(2):321–361. https://doi.org/10.1046/j.1365-246X.2002.01627.x
Hamaguchi H, Goto K, Wada Y (1977) Icequakes observed in the Lake Suwa. 3. Relationship between icequakes and temperatures. Abst Spring Meet Seismol Sot Jpn.127
Harada T, Ishibashi K (2000) The 1958 great Etorofu earthquake was a slab event: suggestion from the mainshock-aftershock relocation. EOS 81(22):Suppl. WP157
Harada T, Ishibashi K (2008) Interpretation of the 1993, 2001, and 2002 Guam Earthquakes as intraslab events by a simultaneous relocation of the mainshocks, aftershocks, and background earthquakes. Bull Seismo Soc Am 98(3):1581–1587. https://doi.org/10.1785/0120060227
Hawley WB, Allen RM, Richards MA (2016) Tomography reveals buoyant asthenosphere accumulating beneath the Juan de Fuca plate. Science 353(6306):1406–1408. https://doi.org/10.1126/science.aad8104
Heuret A, Lallemand S (2005) Plate motions, slab dynamics and back-arc deformation. Phys Earth Planet Int 149(1–2):31–51. https://doi.org/10.1016/j.pepi.2004.08.022
Huang Z, Zhao D, Hasegawa A, Umino N, Park J-H, Kang I-B (2013) Aseismic deep subduction of the Philippine sea plate and slab window. J Asian Earth Sci 75:82–94. https://doi.org/10.1016/j.jseaes.2013.07.002
Isacks B, Molnar P (1971) Distribution of stresses in the descending lithosphere from a global survey of focal-mechanism solutions of mantle earthquakes. Rev Geophys 9(1):103–174. https://doi.org/10.1029/RG009i001p00103
Ishii K, Wallis SR (2022) A possible mechanism for spontaneous cyclic back-arc spreading. Prog Earth Planet Sci 9(1):27. https://doi.org/10.1186/s40645-022-00486-3
Lallemand S, Heuret A, Boutelier D (2005) On the relationships between slab dip, back-arc stress, upper plate absolute motion, and crustal nature in subduction zones. Geochem Geophys Geosyst 6(9):Q09006. https://doi.org/10.1029/2005GC000917
Lallemand S, Heuret A, Faccenna C, Funiciello F (2008) Subduction dynamics as revealed by trench migration. Tectonics 27(3):TC3014. https://doi.org/10.1029/2007TC002212
Li C, van der Hilst RD, Engdahl ER, Burdick S (2008) A new global model for P wave speed variations in earth's mantle. Geochem Geophys Geosyst 9:Q05018. https://doi.org/10.1029/2007GC001806
Mallick R, Parameswaran RM, Rajendran K (2017) The 2005 and 2010 earthquakes on the Sumatra-Andaman trench: evidence for post-2004 megathrust intraplate rejuvenation. Bull Seismo Soc Am 107(4):1569–1581. https://doi.org/10.1785/0120160147
McCaffrey R (2008) Global frequency of magnitude 9 earthquakes. Geology 36(3):263–266. https://doi.org/10.1130/G24402A.1
Obrebski M, Allen RM, Xue M, Hung S-H (2010) Slab-plume interaction beneath the Pacific Northwest. Geophys Res Lett 37(14):L14305. https://doi.org/10.1029/2010GL043489
Preston LA, Creager KC, Crosson RS, Brocher TM, Trehu AM (2002) Intraslab earthquakes: dehydration of the Cascadia slab. Science 302(5648):1197–1200. https://doi.org/10.1126/science.1090751
Schellart WP, Stegman DR, Freeman J (2008) Global trench migration velocities and slab migration induced upper mantle volume fluxes: constraints to find an earth reference frame based on minimizing viscous dissipation. Earth-Sci Rev 88(1–2):118–144. https://doi.org/10.1016/j.earscirev.2008.01.005
Seno T, Yoshida M (2004) Where and why do large shallow intraslab earthquakes occur? Phys Earth Planet Int 141(3):183–206. https://doi.org/10.1016/j-pepi.2003.11.002
Sippl C, Dielforder A, John T, Schmalholz SM (2022) Global constraints on intermediate-depth intraslab stresses from slab geometries and mechanisms of double seismic zone earthquakes. Geochem Geophys Geosyst 23(9):e2022GC010498. https://doi.org/10.1029/2022GC010498
Steinberger B, Sutherland R, O'Connell RJ (2004) Prediction of Emperor-Hawaii seamount locations from a revised model of global plate motion and mantle flow. Nature 430:167–173. https://doi.org/10.1038/nature02660
Tajima F, Yoshida M, Ohtani E (2015) Conjecture with water and rheological control for subducting slab in the mantle transition zone. Geosci Front 6(1):79–93. https://doi.org/10.1016/j.gsf.2013.12.005
Utsu T (1972) Large earthquakes near Hokkaido and the expectancy of the occurrence of a large earthquake off Nemuro. Rep Coord Comm Earthq Predict 7:7–13
Utsu T (1982) Tables of earthquakes with magnitude 6.0 or larger and earthquakes associated with damage near Japan: 1885–1980. Bull Earthq Res Inst 57:401–463
Uyeda S, Kanamori H (1979) Back-arc opening and the mode of subduction. J Geophys Res 84(B3):1049–1061. https://doi.org/10.1029/JB084iB03p01049
Wang L, Dai L, Gong W, Li S, Jiang X, Foulger G, Dong H, Li Z-H, Yu S (2022) Subduction initiation at the Solomon back-arc basin: contributions from both island arc rheological strength and oceanic plateau collision. Geophys Res Lett 49(3):e2021GL093369. https://doi.org/10.1029/2021GL097666
Wessel P, Smith WHF, Scharroo R, Luis JF, Wobbe F (2013) Generic mapping tools: improved version released. EOS Trans AGU 94(45):409–410. https://doi.org/10.1002/2013EO450001
Wong IG (2005) Low potential for large intraslab earthquakes in the central Cascadia subduction zone bull. Seismo Soc Am 95(5):1880–1902. https://doi.org/10.1785/0120040132
Ye L, Lay T, Bai Y, Cheung KF, Kanamori H (2017) The 2017 Mw 8.2 Chiapas, Mexico, earthquake: energetic slab detachment. Geophys Res Lett 44(23):11824–11832. https://doi.org/10.1002/2017GL076085
Yoshida M (2013) The role of harzburgite layers in the morphology of subducting plates and the behavior of oceanic crustal layers. Geophys Res Lett 40(20):5387–5392. https://doi.org/10.1002/2013GL057578
Yoshida M (2017) Trench dynamics: effects of dynamically migrating trench on subducting slab morphology and characteristics of subduction zones systems. Phys Earth Planet Int 268:35–53. https://doi.org/10.1016/j.pepi.2017.05.004
Zahirovic S, Seton M, Müller RD (2014) The cretaceous and cenozoic tectonic evolution of Southeast Asia. Solid Earth 5:227–273. https://doi.org/10.5194/se-5-227-2014
Zhao D (2015) Multiscale seismic tomography. Springer Japan, Tokyo, p 304

Publisher's Note